MECHANICAL PROPERTIES AND ACOUSTIC EMISSION CHARACTERISTICS OF GRANITE UNDER THERMO-HYDRO-MECHANICAL COUPLING

by

Xin-Zhong WANG [a,b], ***Dong WANG*** [b,c,d], ***Zhe-Wei WANG*** [d], ***Xiao-Juan YIN*** [d], ***Xue-Jun ZHOU*** [d], ***Ru ZHANG*** [b,c*], ***An-Lin ZHANG*** [a,b], ***Gan FENG*** [a,b], ***and Li REN*** [c*]

[a] State Key Laboratory of Hydraulics and Mountain River Engineering, Sichuan University, Chengdu, China
[b] College of Water Resource and Hydro Power, Sichuan University, Chengdu, China
[c] MOE Key Laboratory of Deep Earth Science and Engineering, Sichuan University, Chengdu, China
[d] China Railway Eryuan Engineering Group Company, Ltd., Chengdu, China

Original scientific paper
https://doi.org/10.2298/TSCI2106585W

Exploring the mechanical properties and thermal cracking characteristics of rock under thermo-hydro-mechanical coupling in detail is of great importance for the safe excavation and stability of deep rock engineering. The mechanical properties and thermal cracking characteristics of granite under burial depths of 1000 m (confining pressure of 25 MPa) and 1600 m (confining pressure of 40 MPa) at a temperature of 110 °C and a pore water pressure of 10 MPa were studied.The results show that the elastic modulus decreases with increasing temperature under a confining pressure of 25 MPa, whereas under a confining pressure of 40 MPa, the elastic modulus increases with increasing temperature. As the pore water pressure increases, the elastic modulus decreases slightly. Poisson's ratio increases with increasing temperature below 40 °C but decreases from 50-110 °C. Poisson's ratio increases as pore water pressure increases. During the heating process, acoustic emission activity is first detected at 30-40 °C and is relatively stable from 40-90 °C. The acoustic emission activity increases sharply at 90-110 °C, and the thermal cracking threshold of granite under thermo-hydro-mechanical coupling is approximately 95 °C.

Key words: *thermo-hydro-mechanical coupling, granite, mechanical properties, thermal cracking*

Introduction

The study of the mechanical properties of rocks under thermo-hydro-mechanical (THM) coupling is of great importance, as THM processes are relevant to the design, construction, operation and safety assessment of deep and long mountain tunnels and other deep geotechnical engineering works, such as deep mineral development, radioactive waste storage and geothermal energy extraction [1, 2]. The mechanical properties of rocks are altered by THM processes, causing multiple changes [2]:

– The physical and mechanical properties, fluid-flow characteristics and stress distribution of rocks change with temperature.

* Corresponding authors, e-mail: zhangru@scu.edu.cn, renli-scu@hotmail.com

– Pore pressure effects change the stress field and reduce the strength of the surrounding rock where the local permeability, heat conduction and convection have been altered.
– Induced stresses cause the initiation and propagation of cracks in the rock mass, altering its internal heat conduction and hydraulic conductivity.

Research on the variations in the physical and mechanical properties of rocks with temperature has considered mainly the effect of high temperatures due to interest in the surrounding rock stability of radioactive waste storage and geothermal energy extraction [3, 4]. Many previous studies of the effect of water on the physical and mechanical properties of rocks aimed to investigate the effects of certain factors, such as the pore water pressure, saturation or content, or the coupled effects of the hydrothermal (HT) and hydromechanical (HM) processes [5-7]. However, the variation in the physical and mechanical properties of rock under THM coupling has not been fully revealed. It is necessary to further explore to ensure the stability of deeply buried long tunnels in a multifield coupled environment.

Acoustic emission (AE) is a transient elastic wave phenomenon produced by energy released from rock and other materials in the process of crack initiation and growth under external loading [8]. Extensive research on the spatio temporal evolution, fractal characteristics and damage evolution of AE events has been conducted under varying loading conditions, such as uniaxial compression, triaxial compression, cyclic loading and unloading and multifield coupling [9-12]. Similarly, the micro-cracks in rock are reactivated during heating. This thermal cracking produces AE. Hence, it is appropriate to explore the thermal cracking characteristics of rock under THM coupling with AE monitoring.

Studying thermal cracking characteristics and the change in mechanical properties under THM coupling can provide a better reference for the stability study of deep and long tunnels. In this study, two burial depths of deep tunnels or underground chambers, *i.e.*, 1000 m (confining stress of 25 MPa) and 1600 m (confining stress of 40 MPa) were selected to study the mechanical properties and thermal cracking characteristics of granite at 110 °C and a pore water pressure of 10 MPa. Loading and unloading tests of granite under THM coupling in the elastic stage of rock deformation were designed and implemented. With this test method, only one rock sample is needed to obtain the variation laws of mechanical parameters with temperature and pore water pressure, which can save time and avoid the influence of the differences among samples on the test results. The AE recordings were obtained during heating to explore the thermal cracking characteristics and ascertain the thermal cracking threshold under THM coupling.

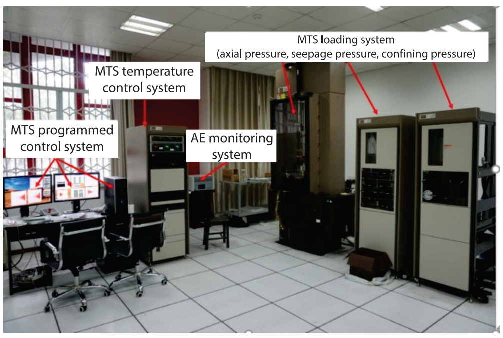

Figure 1. Rock mechanics experimental testing and AE monitoring system under THM coupling

Coupled THM testing of granite

Description of rock samples and testing facilities

Granite samples were collected from the Chengdu-Tibet section of the No. 318 national highway in China. Rock samples were processed into cylindrical samples (100 mm high × 50 mm in diameter), following ISRM standards. Before the experiments, the rock samples were saturated with water under vacuum. The loading and unloading tests of the elastic stage under THM coupling were carried out using an MTS815 Flex Test GT mechanical test system at Sichuan University, and the

PCI-2 AE system manufactured by the Physical Acoustic Corporation (PAC) was used to record the time sequence and spatial location of AE events during the heating process, as shown in fig. 1. The MTS815 Flex Test GT system is capable of supplying a maximum confining stress of 140 MPa, a maximum pore water pressure of 140 MPa, and a maximum axial load of 4600 kN and heating samples to temperatures up to 200 °C. The maximum signal amplitude of the PCI-2 AE system is 100 dB, and the dynamic range exceeds 85 dB.

Testing method

In this study, two confining pressure levels, four pore water pressure ranges and seven temperature gradients were investigated, as presented in tab. 1.

Table 1. Confining pressure, temperature, and pore water pressure during the loading and unloading testingin the elastic stage of granite under THM coupling

Confining pressure, σ_3 [MPa]	Pore water pressure, P_w [MPa]	Temperature, T [°C]									
25	0.3	20	30	40	50	60	70	80	90	100	110
	3	20	30	40	50	60	70	80	90	100	110
	6	20	30	40	50	60	70	80	90	100	110
	10	20	30	40	50	60	70	80	90	100	110
40	0.3	20	30	40	50	60	70	80	90	100	110
	3	20	30	40	50	60	70	80	90	100	110
	6	20	30	40	50	60	70	80	90	100	110
	10	20	30	40	50	60	70	80	90	100	110

The detailed test process was:

Step 1. The initial test temperature, T, was the ambient temperature (20 °C). The saturated samples were loaded hydrostatically up to a predetermined confining pressure σ_3, which was maintained for the remainder of the test.

Step 2. A pore water pressure, P_w, was applied at the top and bottom of the specimen until the target value was reached.

Step 3. The axial deviatoric stress was loaded to 30 MPa at a confining stress of 25 MPa (60 MPa at a confining stress of 40 MPa) and then unloaded.

Step 4. The P_w was regulated to reach the next target value.

Step 5. Steps 3 and 4 were repeated until the loading and unloading tests of the elastic stage were completed under all the pore water pressure conditions at the set temperature.

Step 6. The rock sample was heated at a rate of 1 °C per minute to reach the next target temperature while maintaining a constant P_w of 10 MPa.

Step 7. Steps 3 and 4 were repeated until the loading and unloading tests of the elastic stage were completed under all the temperature conditions.

The aforementioned test steps are represented by the flow charts in fig. 2. As shown in fig. 2, the blue dot represents the predetermined testing conditions, and the green and red arrows indicate the changing pore water pressure and temperature, respectively.

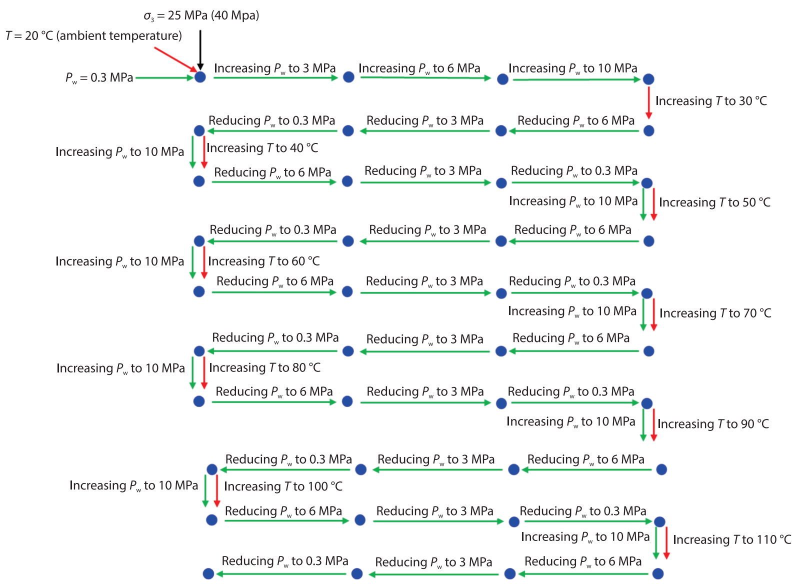

Figure 2. Schematic diagram of the loading and unloading test scheme of granite in the elastic stage under THM coupling

Results and analysis

Stress–strain curves of rock samples under THM coupled

Under the loading and unloading tests of the granite samples with THM coupling, these experimental processes, such as applying a confining pressure, heating, applying a pore water pressure, and axial loading and unloading within the elastic stage, may affect the mechanical properties of rock. The AE is a phenomenon of strain energy release in the form of elastic waves when a material is fractured and damaged. The AE characteristics of these four stages of testing can directly reflect the extent of their influence on the mechanical properties of rock samples. The statistical results of the AE monitoring in the four stages of testing are listed in tab. 2.

Table 2. Statistical results of AE monitoring in the four stages of testing

Confining pressure	Application of confining pressure	Application of pore water pressure	Heating stage	Loading and unloading process
25	4	0	61	0
40	5	4	49	0

Table 2 shows that during the whole test, the mechanical properties of the rock are mainly affected by the heating process under THM coupling. The influence of the application of pore water pressure and the loading and unloading process within the elastic stage is relatively weak and can be neglected. Hence, it is appropriate to study the mechanical properties and thermal cracking characteristics of loading and unloading experiments within the elastic stage under THM coupling.

Through the loading and unloading testing of two samples in the elastic deformation stage under THM coupling, the loading and unloading stress-strain curves of the elastic deformation section with confining pressures of 25 MPa and 40 MPa were obtained. Due to the limited length of this paper, the stress-strain curves of some testing results are shown in fig 3. The loading and unloading curves of the rock samples are basically linear in fig. 3, indicating that the deformation of the rock samples remained in the elastic stage, so it is reasonable to calculate the mechanical parameters of the elastic deformation of a rock sample via the corresponding loading and unloading curve.

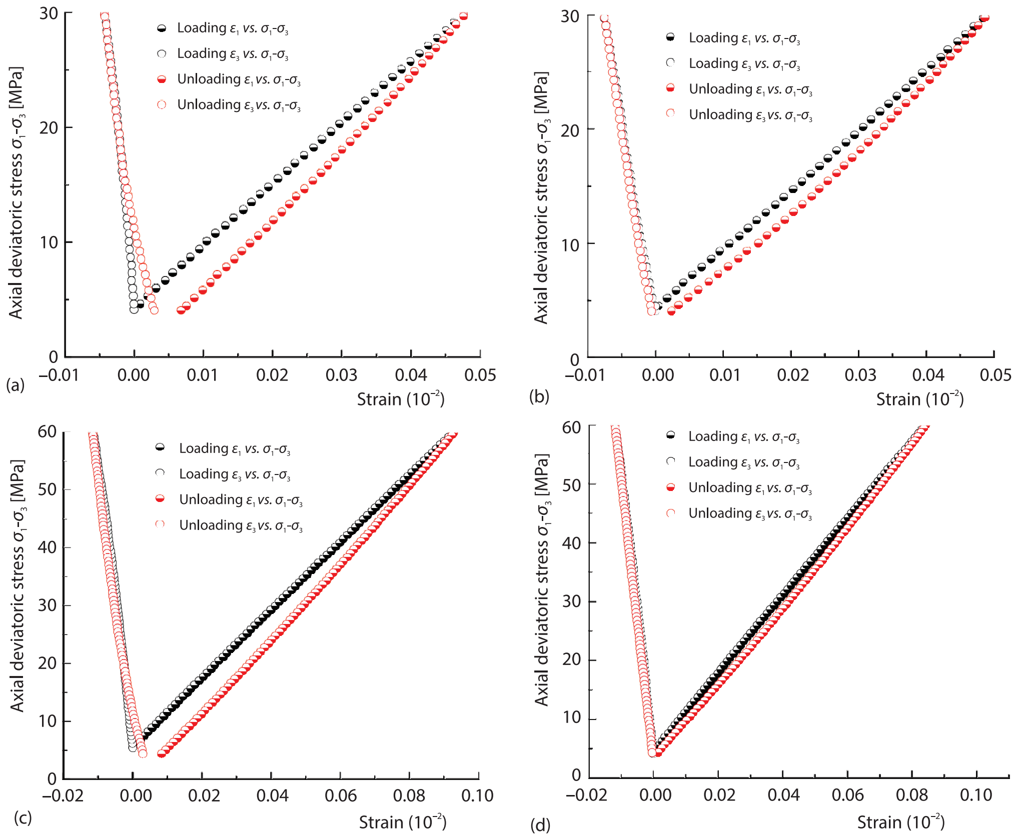

Figure 3. The loading and unloading stress-strain curves of the elastic deformation stage of graniteunder THM coupling; (a) σ_3 = 25 MPa, T = 20 °C, P_w = 0.3 MPa, (b) σ_3 = 25 MPa, T = 100 °C, P_w = 10 MPa, (c) σ_3 = 40 MPa, T = 20 °C, P_w = 0.3 MPa, and (d) σ_3 = 40 MPa, T = 100 °C, P_w = 10 MPa

Variations in elastic modulus

Obtaining the elastic modulus and Poisson's ratio of rock is the premise of rock engineering design and stability analysis. The elastic modulus of granite was calculated by linear fitting using the data of the approximately linear section of the stress-strain curve during the elastic unloading stage. The elastic modulus and Poisson's ratio read [13]:

$$E = \frac{\sigma_1 - 2\mu\sigma_3}{\varepsilon_1} \tag{1}$$

and

$$\mu = \frac{B\sigma_1 - \sigma_3}{\sigma_3(2B-1) - \sigma_1}, \quad B = \frac{\varepsilon_3}{\varepsilon_1} \tag{2}$$

where E is the elastic modulus, μ – the Poisson's ratio, σ_1– the axial stress, σ_3 – the confining pressure, ε_2 – the axial strain, and ε_3 – the lateral strain. By normalizing the elastic modulus and Poisson's ratio, variations of the relative values of elastic modulus and Poisson's ratio with temperature and pore water pressure can be obtained:

$$F_1 = \frac{E_\mathrm{T} - E_{\mathrm{T}_0}}{E_{\mathrm{T}_0}}, \quad F_2 = \frac{E_\mathrm{P} - E_{\mathrm{P}_0}}{E_{\mathrm{P}_0}} \tag{3}$$

$$F_3 = \frac{\mu_T - \mu_{T_0}}{\mu_{T_0}}, \quad F_4 = \frac{\mu_P - \mu_{P_0}}{\mu_{P_0}} \tag{4}$$

where E_T is the average value of elastic modulus at different temperatures, E_P – the average value of elastic modulus at different pore water pressures, E_{T0} – the average value of elastic modulus at room temperature, E_{P0} – the average value of elastic modulus at pore water pressures of 0.3 MPa, μ_T – the average value of Poisson's ratio at different temperatures, μ_P – the average value of Poisson's ratio at different a pore water pressures, μ_{T_0} – the average value of Poisson's ratio at room temperature, μ_{p_0} – the average value of elastic modulus at a pore water pressures of 0.3 MPa, F_1 – the variation coefficient of elastic modulus with temperature, F_2 – the variation coefficient of elastic modulus with pore water pressure, F_3 – the variation coefficient of Poisson's ratio with temperature, and F_4 – the the variation coefficient of Poisson's ratio with pore water pressure.

For a confining pressure of 25 MPa, the variations in the elastic modulus with temperature and pore water pressure are shown in fig. 4. Under a confining pressure of 25 MPa, the elastic modulus decreases with increasing temperature. The elastic modulus changes little with increasing temperature below 30 °C, while it decreases to a certain extent by 40 °C. At 50 °C, the elastic modulus is slightly higher than that at 40 °C. From 50-100 °C, the elastic modulus decreases linearly, but the reduction is small. At 110 °C, the elastic modulus decreases significantly. Under a confining pressure of 25 MPa, there are two temperature thresholds at which the elastic modulus decreases with increasing temperature, which are 40 °C and 110 °C, corresponding to decreases of 7.2% and 17.4%, respectively, compared with the elastic modulus measured at room temperature (20 °C).

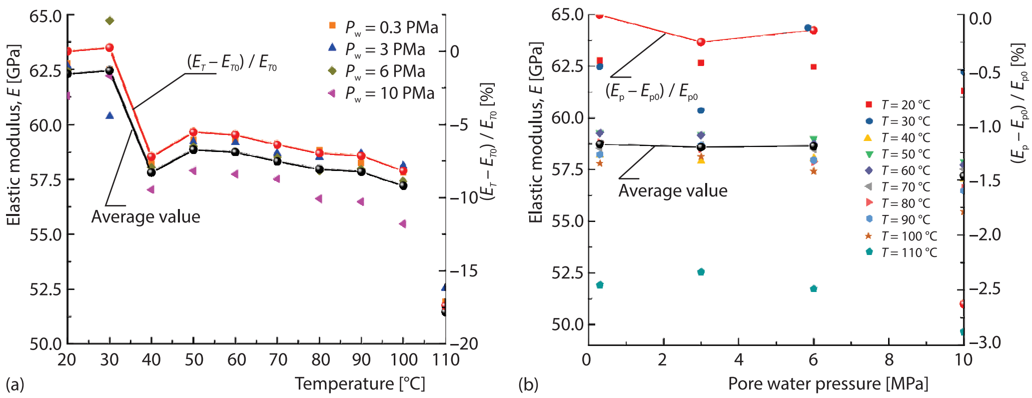

Figure 4. Variations inelastic modulus with temperature and pore water pressure under a confining pressure of 25 MPa; (a) *E vs. T* and (b) *E vs. P_w*

Under a confining pressure of 25 MPa, when the pore water pressure is less than 6 MPa, the elastic modulus does not change obviously. When the pore water pressure is

10 MPa, the elastic modulus is 2.6% lower that under a pore water pressure of 0.3 MPa. When the confining pressure is 40 MPa, variations in the elastic modulus with temperature and pore water pressure are plotted in fig. 5. Below 30 °C, the elastic modulus increases with the temperature, while it does not change considerably from 30-40 °C. From 50-70 °C, the elastic modulus decreases slightly. From 70-110 °C, the elastic modulus increases linearly. Under a confining pressure of 40 MPa, the two temperature thresholds at which the elastic modulus increases with temperature are 40 °C and 110 °C, which are 2.0% and 4.4% lower than those at 20 °C. Under a confining pressure of 40 MPa, when the pore water pressure is less than 3 MPa, the elastic modulus does not change significantly. When the pore water pressure increases from 3-10 MPa, the elastic modulus decreases linearly with increasing pore water pressure, but the reduction is small.

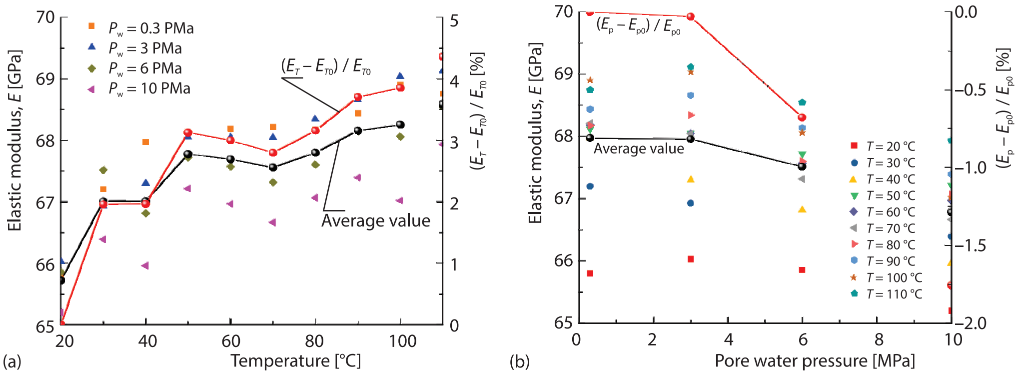

Figure 5. Variations inelastic modulus with temperature and pore water pressure under a confining pressure of 40 MPa; (a) *E vs. T* and (b) *E vs.* P_w

A comparison of figs. 4 and 5 indicates that the influences of confining pressures of 25 MPa and 40 MPa on the elastic modulus of granite are very different, indicating that the confining pressure will affect the deterioration characteristics of the rock mechanical properties. The confining pressure constrains the thermal expansion of rock and reduces the influence of thermal cracking on rock deterioration. A high confining pressure greatly constrains the thermal expansion of rock, which may lead to rock compaction and increase the elastic modulus of rock to a certain extent. The elastic modulus decreases with increasing pore water pressure, indicating that the pore water pressure mainly affects the elastic modulus of rock by reducing the effective confining pressure on the rock skeleton. The pore water pressures applied in the test were relatively low, so the effective confining pressure of the rock did not decrease greatly, and the elastic modulus did not decrease significantly.

Variations in Poisson's ratio

Variations in Poisson's ratio with temperature and pore water pressure are shown in fig. 6 for a confining pressure of 25 MPa. Under a confining pressure of 25 MPa and increasing temperature, Poisson's ratio increases below 30 °C, decreases from 30-60 °C, increases slightly from 60-90 °C, and decreases from 90-110 °C. When the temperature is below 110 °C, Poisson's ratio is slightly higher than that at room temperature. When the confining pressure is 25 MPa, Poisson's ratio increases when the pore water pressure increases from 0.3 MPa to 6 MPa and decreases slightly when the pore water pressure is 10 MPa. Variations in Poisson's ratio with temperature and pore water pressure are plotted in fig. 7 for a confining pressure in 40 MPa. Under a confining pressure of 40 MPa, the Poisson's ratio at 30 °C is equal to that at room temperature. At 40 °C, Poisson's ratio increases slightly with temperature. From 40-90 °C, Poisson's ratio decreases with increasing temperature. From 90-110 °C, Poisson's ratio changes little. When the confining pressure is 40 MPa, Poisson's ratio increases when the pore water pressure increases from 0.3-6 MPa. When the pore water pressure is 10 MPa, Poisson's ratio is approximately equal to that under apore water pressure of 6 MPa.

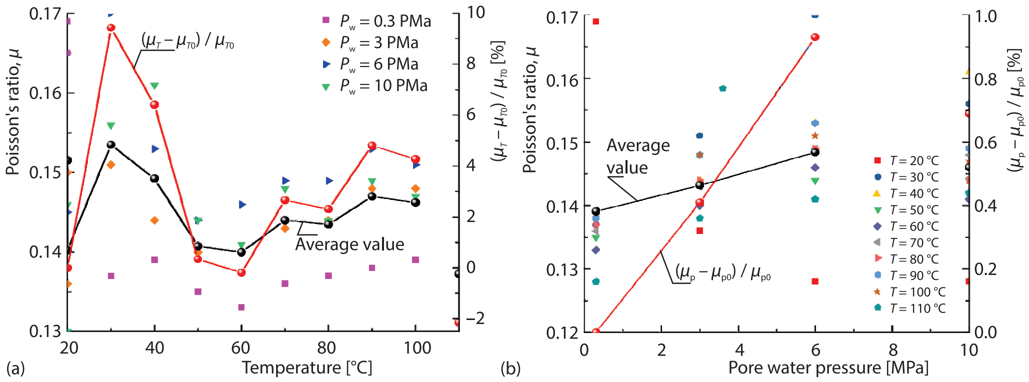

Figure 6. Variations in Poisson's ratio with temperature and pore water pressure under a confining pressure of 25 MPa; (a) μ *vs.* T and (b) μ *vs.* P_w

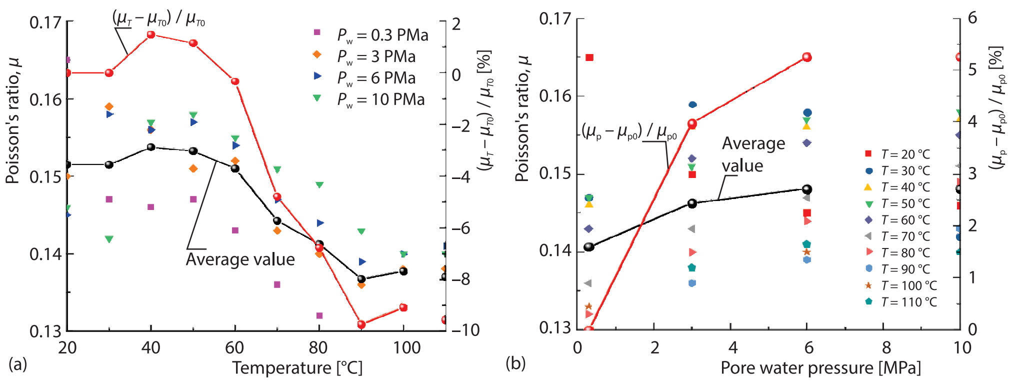

Figure 7. Variations in Poisson's ratio with temperature and pore water pressure under a confining pressure of 40 MPa; (a) μ *vs.* T and (b) μ *vs.* P_w

According to the comparison between figs. 6 and 7, Poisson's ratio at 25 MPa increases by 9.4% compared with that at room temperature, and Poisson's ratio decreases by 2.1% at 110 °C. Under a confining pressure of 40 MPa, Poisson's ratio increases by 1.5% at 40 °C and decreases by 9.6% at 110 °C. This indicates that increasing the temperature leads to an increase in the lateral deformation ability of the rock. However, the high confining pressure constrains the thermal expansion of rock and thus the lateral deformation of the rock, leading to a decrease in Poisson's ratio. Under confining pressures of 25 MPa and 40 MPa, Poisson's ratio increases as the pore water pressure increases. This is because the pore water pressure increases mainly the lateral deformation of the rock by reducing the effective pressure on the rock skeleton. When the confining pressure is 25 MPa, Poisson's ratio increases by less than 1% when the pore water pressure is 10 MPa, however, when the confining pressure is 40 MPa, Poisson's ratio increases by 5.3% under a pore water pressure of 10 MPa. This indicates that the lateral deformation of rock is more easily affected by the pore water pressure under a higher confining pressure.

The AE characteristics of micro cracking induced under THM coupling

The AE characteristic parameters, such as AE counts and AE energy, were selected to explore the thermal cracking mechanism under THM coupling. The normalized AE counts and AE energy can be determined:

$$G_1 = \frac{N}{N_C}, \quad G_2 = \frac{U}{U_C} \tag{5}$$

where N and U are the cumulative AE counts and cumulative AE energy at a certain temperature, N_C and U_C – the cumulative AE counts and cumulative AE energy during the whole heating process, G_1 – the cumulative AE counts normalization index, and G_2 – the cumulative AE energy normalization index. The evolution of AE characteristic parameters of granite over time during heating under a confining pressure of 25 MPa and a pore water pressure of 10 MPa is shown in fig. 8. The evolution of the AE characteristic parameters of granite with time during heating under a confining pressure of 40 MPa and a pore water pressure of 10 MPa is shown in fig. 9. The variations in the AE characteristic parameters of granite with confining pressure and temperature are:

- Weak AE signals are detected during the application of the confining pressure due to the compaction of the micro-cracks in the granite.
- The AE signals are first detected at 30-40 °C: with the limitation of the effective confining pressure (coupled effect of confining pressure and pore water pressure), the original fractures in the granite close at this temperature, leading to AE. This result is similar to Zhang *et al.* [14] conclusion obtained from the AE characteristics of granite observed during the heating process under a confining pressure of 20 MPa.
- From 40-90 °C, the internal micro-cracks of the rock samples basically close, and the thermal stress is not enough to cause significant thermal fracturing of the rock. Hence, in this temperature range, the AE phenomenon caused by thermal cracking is not severe, and the variation in AE characteristic parameters is relatively stable.
- From 90-110 °C, especially at approximately 95 °C, the number of AE events in and the amount of energy released from the rock samples increase sharply, which indicates that due to the difference in the thermal expansion and anisotropy of the thermal expansion of mineral particles in rock, the stress acting on the boundary of the mineral particles satisfies eq. (6) [15], exceeding strength limit, inducing microfracture of rock and the release of internal accumulated strain energy:

$$\sigma_{\mathrm{m}} \geq \frac{4\gamma E\sqrt{d}}{K\left(1+\mu\right)} \tag{6}$$

where σ_{m} is the stress acting on the boundary of the mineral particles, γ – the surface energy, d – the size of mineral particles, and K – the yield constant.

The results of the coupled THM testing conducted in this work indicate that the thermal cracking threshold of granite is 95 °C, this finding is similar to the 90 °C thermal cracking threshold of granite observed under a confining pressure of 20 MPa [14], higher than the 60-70 °C thermal cracking threshold of Westerly granite obtained by Chen *et al*. [16], and lower than the 120 °C thermal cracking threshold of Luhui granite obtained by Wu *et al*. [17]. Notably, these thermal cracking threshold results may vary due to the different mineral compositions of the selected rock samples and different test conditions.

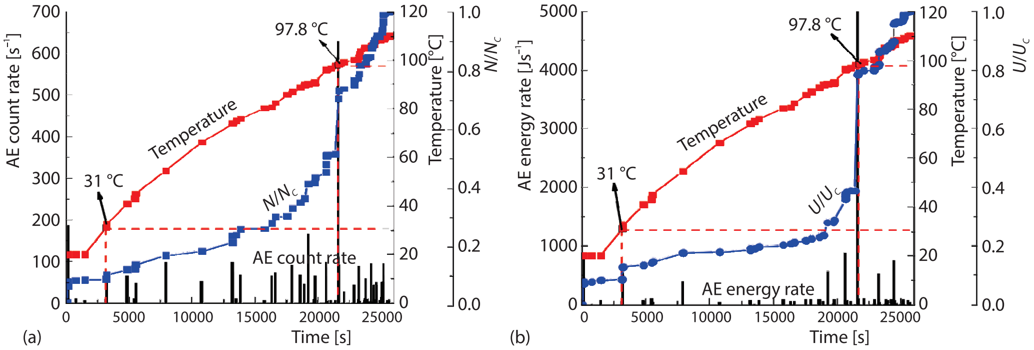

Figure 8. Variation in AE characteristic parameters of granite with time during heating (confining pressure of 25 MPa, pore water pressure of 10 MPa); (a) AE counts and (b) AE energy

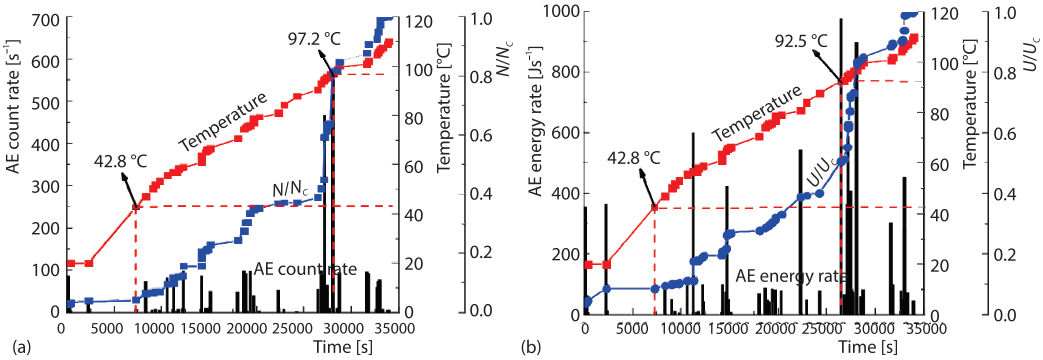

Figure 9. Variation in AE characteristic parameters of granite with time during heating (confining pressure of 40 MPa, pore water pressure of 10 MPa); (a) AE counts and (b) AE energy

Conclusions

Through the loading and unloading testing of the elastic deformation stage of granite under THM coupling in this study, variations in the physical and mechanical parameters of granite with temperature and pore water pressure were studied. The thermal fracture characteristics of granite during heating were studied by AE monitoring technology. The elastic modulus decreases with increasing temperature under a confining pressure of 25 MPa and decreases by 17.4% at 110 °C compared with the ambient temperature (20 °C). Under a confining pressure of 40 MPa, the elastic modulus increases with temperature and increases by 4.3% at 110 °C compared with ambient temperature. The elastic modulus decreases as the pore water pressure increases, but the influence of pore water pressure on the elastic modulus is small. Poisson's ratio first increases and then decreases as the temperature increases. Under a confining pressure of 25 MPa, the Poisson's ratio at 30 °C is 9.4% higher than that at the ambient temperature, and that at 110 °C is 2.1% lower than that at the ambient temperature. Under a confining pressure of 40 MPa, the Poisson's ratio at 40 °C is 1.5% higher than that at the ambient temperature, and that at 110 °C is 9.6% lower than that at the ambient temperature. Poisson's ratio increases with increasing pore water pressure. The extent of increase in Poisson's ratio under a confining pressure of 40 MPa is greater than that under a confining pressure of 25 MPa. In the heating process under THM coupling, AE activity is first detectedwhen the temperature is 30-40 °C and remains relatively stable from 40-90 °C. The AE ringing count and energy increase abruptly at 90-110 °C. The thermal cracking threshold of granite under THM coupling is approximately 95 °C.

Acknowledgment

Financial supports were provided from the Key R and D projects of Sichuan Science and Technology Plan under Grant No. 19YFG0047, and the Research project of China Railway Eryuan Engineering Group Company, Ltd under Grant No. 19H0537, and China Postdoctoral Science Foundation (Grant No. 2020M673225), and we are gratefully acknowledged.

Nomenclature

d – size of mineral particles, [mm]
E – elastic modulus, [GPa]
K – yield constant, [MPa]
P_w – pore water pressure, [MPa]
T – temperature,[°C]

Greek symbols

γ – surface energy, [Jmm^{-2}]
ε_1 – axial strain, [–]
ε_3 – lateral strain, [–]
μ – Poisson's ratio, [–]
σ_1 – axial stress, [MPa]
σ_3 – confining pressure, [MPa]

References

[1] Pan, P. Z., *et al*. Coupled THM Processes in EDZ of Crystalline Rocks Using an Elasto-Plastic Cellular Automaton, *Environmental Geology*, *57* (2008), 6, pp. 1299-1311
[2] Nasseri, M. H. B., *et al*., Thermo-Hydro-Mechanical Properties of Cobourg Limestone, *International Journal of Rock Mechanics and Mining Sciences*, *61* (2013), Complet, pp. 212-222
[3] Mahanta, B., *et al*., Influence of Thermal Treatment on Mode I Fracture Toughness of Certain Indian Rocks, *Engineering Geology*, *210* (2016), 5, pp. 103-114
[4] Brotons, V., *et al*., Temperature Influence on the Physical and Mechanical Properties of a Porous Rock: San Julian's Calcarenite, *Engineering Geology*, *167* (2013), Dec., pp. 117-127
[5] Ghabezloo, S., *et al*., Effective Stress Law for the Permeability Of a Limestone, *International Journal of Rock Mechanics and Mining Sciences*, *46* (2009), 2, pp. 297-306
[6] Lion, M., *et al*., Effects of Heating on the Hydraulic and Poroelastic Properties of Bourgogne Limestone, *International Journal of Rock Mechanics and Mining Sciences*, *42* (2005), 4, pp. 508-520
[7] Liu, S., *et al*., An Experimental Study on the Physico-Mechanical Properties of Two Post-High-Temperature Rocks, *Engineering Geology*, *185* (2015), 5, pp. 63-70
[8] Jia, Z. Q., *et al*., Acoustic Emission Characteristics and Damage Evolution of Coal at Different Depths under Triaxial Compression, *Rock Mechanics and Rock Engineering*, *53* (2020), 5, pp. 2063-2076
[9] Kong, B., *et al*. Non-linear Characteristics of Acoustic Emissions During the Deformation and Fracture of Sandstone Subjected to Thermal Treatment, *International Journal of Rock Mechanics and Mining Sciences*, *90* (2016), Jan., pp. 43-52
[10] Zhou, H. W., *et al*., On Acoustic Emission and Post-peak Energy Evolution in Beishan Granite under Cyclic Loading, *Rock Mechanics and Rock Engineering*, *52* (2018), 1, pp. 283-288
[11] Ai, T., *et al*., Space-Time Evolution Rules of Acoustic Emission Location of Unloaded Coal Sample at Different Loading Rates, *International Journal of Mining Science and Technology*, *22* (2012), 6, pp. 847-854
[12] Yang, S. Q., *et al*., Spatial Acoustic Emission Evolution of Red Sandstone during Multi-Stage Triaxial Deformation, *Journal of Central South University*, *21* (2014), 8, pp. 3316-3326
[13] Zhang, Z. P., Differences of Coal Mechanical Parameters and Mining-Induced Mechanical Behavior Induced by Different Depths, Ph. D. thesis, Sichuan University, Chengdu, China, 2019
[14] Zhang, R., *et al*., *Basic Theory and Experimental Research of Rock Acoustic Emission*, Sichuan University Press., Chengdu, China, 2017
[15] Zhang, Z. P., *et al*., Differences in the Acoustic Emission Characteristics of Rock Salt Compared with Granite and Marble during the Damage Evolution Process, *Environmental Earth Sciences*, *73* (2015), 11, pp. 6987-6999

[16] Chen, Y., *et al*., Thermally Induced Acoustic Emission in Westerly Granite, Geophysical Research Letters, *7* (1980), 12, pp. 1089-1092
[17] Wu, J. W., *et al*., Experimental Study of Acoustic Emission Characteristics of Granite Thermal Cracking under Middle-High Temperature and Triaxial Stress, *Rock and Soil Mechanics*, *30* (2009), 11, pp. 3331-3336

Paper submitted: April 11, 2021
Paper revised: June 10, 2021
Paper accepted: July 12, 2021